Computers and Electronics in Agriculture 174 (2020) 105457

Contents lists available at ScienceDirect

Computers and Electronics in Agriculture

journal homepage: www.elsevier.com/locate/compag

Agroview: Cloud-based application to process, analyze and visualize UAV-collected data for precision agriculture applications utilizing artificial intelligence

Yiannis Ampatzidis*, Victor Partel, Lucas Costa

Agricultural and Biological Engineering Department, Southwest Florida Research and Education Center, University of Florida, IFAS, 2685 SR 29 North, Immokalee, FL 34142, USA

ARTICLE INFO

Keywords:
UAVs
Artificial intelligence
Machine learning
Smart agriculture
Precision agriculture
Neural networks
Cloud computing

ABSTRACT

Traditional sensing technologies in specialty crops production, for pest and disease detection and field phenotyping, rely on manual sampling and are time consuming and labor intensive. Since availability of personnel trained for field scouting is a major problem, small Unmanned Aerial Vehicles (UAVs) equipped with various sensors can simplify the surveying procedure, decrease data collection time, and reduce cost. To accurate and rapidly process, analyze and visualize data collected from UAVs and other platforms (e.g. small airplanes, satellites, ground platforms), a cloud and artificial intelligence (AI) based application (named Agroview) was developed. This interactive and user-friendly application can: (i) detect, count and geo-locate plants and plant gaps (locations with dead or no plants); (ii) measure plant height and canopy size (plant inventory); (iii) develop plant health (or stress) maps. In this study, the use of this Agroview application to evaluate phenotypic characteristics of citrus trees (as a case study) is presented. It was found, that this emerging technology detected citrus trees with mean absolute percentage error (MAPE) of 2.3% in a commercial citrus orchard with 175,977 trees (1,871 acres; 39 normal and high-density spacing blocks). Furthermore, it accurately estimated tree height with 4.5% and 12.93% MAPE for normal and high-density spacing respectively, and canopy size with MAPE of 12.9% and 34.6% for normal and high-density spacing respectively. It provides a consistent, more direct, cost-effective and rapid method for field survey and plant phenotyping.

1. Introduction

Precision agriculture aims to optimize resources usage to achieve enhanced agricultural production and reduced environmental impacts (Das, 2018). Assessment of crop growth and timely strategic responses to crop production variations are fundamental challenges in precision agriculture (Panda et al., 2010). In tree crops, measurements of individual tree parameters, such as tree canopy characteristics, are essential to monitor tree growth and optimize orchard management (Maillard and Gomes, 2016). Detecting, counting, and assessing individual trees in orchards allow the selection of appropriate horticultural practices such as the timely application of chemicals and precision irrigation scheduling. Hence, the development of low cost high-throughput phenotyping tools for tree crops is critical and urgent for precision agriculture applications. Traditional sensing technologies for evaluation of field phenotypes rely on manual sampling and are often very labor intensive and time consuming, especially when covering large areas (Mahlein, 2016; Shakoor et al., 2017; Zhang et al., 2019). Additionally, field surveys for pest and disease detection, plant inventory and plant health assessments are expensive, labor intensive and time consuming (Cruz et al., 2019; Partel et al., 2019a; Luvisi et al., 2016).

Remote sensing techniques have been widely applied in precision agriculture for tree crops, utilizing a variety of sensing systems including RGB, multispectral, and hyperspectral imaging, as well as Light Detection and Ranging (LiDAR). RGB and multispectral sensors can be consider as a low-cost systems comparing to hyperspectral and LiDAR. Small unmanned aerial vehicles (UAVs) equipped with RGB and multispectral sensors have recently become flexible and cost-effective solutions for rapid, precise and non-destructive high-throughput phenotyping (Ampatzidis et al., 2017; Pajares, 2015; Singh et al., 2016). UAVs allow growers to constantly monitor crop health status, estimate plant water needs, detect diseases and pests, and quantify pruning strategies and impacts (Abdulridha et al., 2019a,b; Hariharan et al., 2019;

* Corresponding author.
E-mail address: i.ampatzidis@ufl.edu (Y. Ampatzidis).

https://doi.org/10.1016/j.compag.2020.105457
Received 21 February 2020; Received in revised form 22 April 2020; Accepted 22 April 2020

Table 1
Specifications of the UAV-based sensing systems used in this study.

Sensing Systems	Resolution	Pixel resolution at 122 m (400 ft) flight altitude
RGB Zenmuse X5S	5,280 × 3,956 pixels (21 megapixels)	22 × 19 mm
RGB Phantom 4 Pro+	5,472 × 3,648 pixels (19.96 megapixels)	12 × 12 mm

Jiménez-Brenes et al., 2017). They represent a low-cost method for image acquisition in high spatial and temporal resolution, and have been increasingly studied for agricultural applications. Hunt et al. (2010) analyzed UAV multispectral imagery for crop monitoring and found a good correlation between leaf area index and the green normalized difference vegetation index (green NDVI). Matese et al. (2013) mapped the vigor of vineyards using the NDVI index from a high-resolution multispectral camera. Furthermore, UAVs have been utilized to create plant inventories. Malek et al. (2014) achieved promising results in detecting palm trees, by utilizing an extreme learning machine classifier in UAV images. Dong et al. (2020) developed a technique to detect individual apple and pear trees, with 99% and 99.3% F-scores respectively, and to estimate tree-crowns area with a root mean square error of 0.72 m^2 and 0.48 m^2 respectively. Few other efforts have been made to develop UAV-based techniques for tree detection and counting (Salamí et al., 2019), tree height and canopy estimation (Torres-Sánchez et al., 2015; Mu et al., 2018; Fawcett et al., 2019), and tree growth and yield prediction (Jiménez-Brenes et al., 2017; Sarron et al., 2018).

In citrus, remote sensing from UAVs has been utilized to count individual trees (Csillik et al., 2018; Ok and Ozdarici-Ok, 2017), detect HLB (Huanglongbing) and canker affected trees (Abdulridha et al., 2019c; Garcia-Ruiz et al., 2013), and assess tree health/stress (Costa et al., 2020). Romero-Trigueros et al. (2017) analyzed the correlations of citrus physiology stresses and gas exchange status using multispectral images collected by UAVs. Ampatzidis and Partel (2019) developed a UAV-based high throughput phenotyping technique for citrus utilizing artificial intelligence (AI) and machine learning (deep and transfer learning). They utilized this technique for the rapid and efficient evaluation of different citrus cultivars and rootstock varieties in a large-scale commercial field setting (Ampatzidis et al., 2019).

Deep learning and deep convolutional neural networks (CNNs) have been increasingly used in remote sensing for agricultural applications (Kussul et al., 2017; Cruz et al., 2017; Partel et al., 2019b). CNNs require large amount of data to create hierarchical features to provide semantic information at the output (Krizhevsky et al., 2012). With the increasing access to large amounts of aerial images from UAVs and satellites, CNNs can play an important role in processing all these data to obtain valuable information. However, the adoption of UAV-based technologies for specialty crop growers is low (Ghatrehsamani et al., 2018). The main reasons have been based on two fronts. First, the data processing and analysis, in order to generate accurate and useful information, can be very complex and time consuming. Second, the commercially available software provides limited practical information for specialty crops.

Since UAVs can collect a huge and complex amount of data (from a variety of sensors), big data analytics tools and cloud computing can be utilized to increase data processing efficiency, provide data security and scalability, and reduce cost. Cloud-based applications are a solution with low upfront investments, efficient computational resource utilization and usage-based costs (Jinesh, 2011). While standard software must be installed and configured by the user and require maintenance and thus some knowledge of the process, cloud computing eliminates nearly all these concerns. Outsourcing a computation to an internet service also provides advantages in terms of mobility and accessibility (Hayes, 2008). This model allows companies to deploy applications that could scale their computing resources on demand (Villamizar et al., 2016).

This study presents a novel cloud- and AI-based application that can be used to cost-effectively process, analyze, and visualize UAV collected data (from other aerial and ground remote sensing platforms too) to survey and assess agricultural fields. This emerging technology includes a user-friendly and interactive interphase that simplifies the data processing and visualization procedures in order to promote adoption of UAVs and remote sensing for precision agriculture applications. This system was evaluated in a commercial citrus orchards as a case study.

2. Materials and methods

2.1. Data acquisition and sensing platforms

In this study, two quadcopter UAVs (Matrice 210 and Phantom 4 Pro+, DJI, Shenzehen, China) were used for image acquisition. The UAV flight planning and mission control were done by the Pix4DCapture (Pix4D S.A., Prilly, Switzerland) software app used on an iPad (Apple, Cupertino, CA, USA) connected to the remote controller of the UAVs. The quadcopters was equipped with: (i) an RGB (red, green and blue) camera (Zenmuse X5S, DJI, WA, USA), attached to the Matrice 210; (ii) an RGB camera (Phantom 4 Pro + camera, DJI, WA USA), attached to the Phantom 4 Pro + . Table 1 presents the specification of each sensing system.

2.2. Cloud-based software

Several cloud-based computing solutions are commercially available, with one of the options being the Amazon Web Services (AWS) (Amazon, Seattle, Washington, USA), which provides a highly reliable and scalable infrastructure for deploying cloud-based applications (Buyya et al., 2010). The AWS system provides multiple types of instances, machines with different configurations for specific applications, and allow the creation of instance images, copies of all configurations and software on an instance, allowing the use of multiple similar machines.

The application developed in this study uses a general AWS instance (m5a.xlarge) as a main application control machine (with the server to the website), which serves as the user interface to the software. It controls the other instances in the process using the AWS Command Line Interface (CLI). The CLI provides one instance to control the use of other instances in the AWS cloud by sending commands between instances and the cloud.

The stitching engine uses a c5.9xlarge instance for Central Processing Unit (CPU) intensive usage. The tree detection algorithm (which is described below) runs on a p3.2xlarge instance for Graphics Processing Unit (GPU) intensive usage. For scalability and parallel processing, both instances work by creating an image for each process, so the application can receive multiple maps to process at the same time. The data is stored in a Hard Disc Volume unit on the AWS, allowing the allocation of more memory to be upgraded as more data is received.

Upon receiving new data to process, the website activates an image of the engine instance to perform the stitching of the orthomosaic and generate the Digital Surface Model (DSM) file. Once the orthomosaic and DSM files are generated, the CPU image instance is closed. Then, the GPU image instance is activated to perform the tree detection

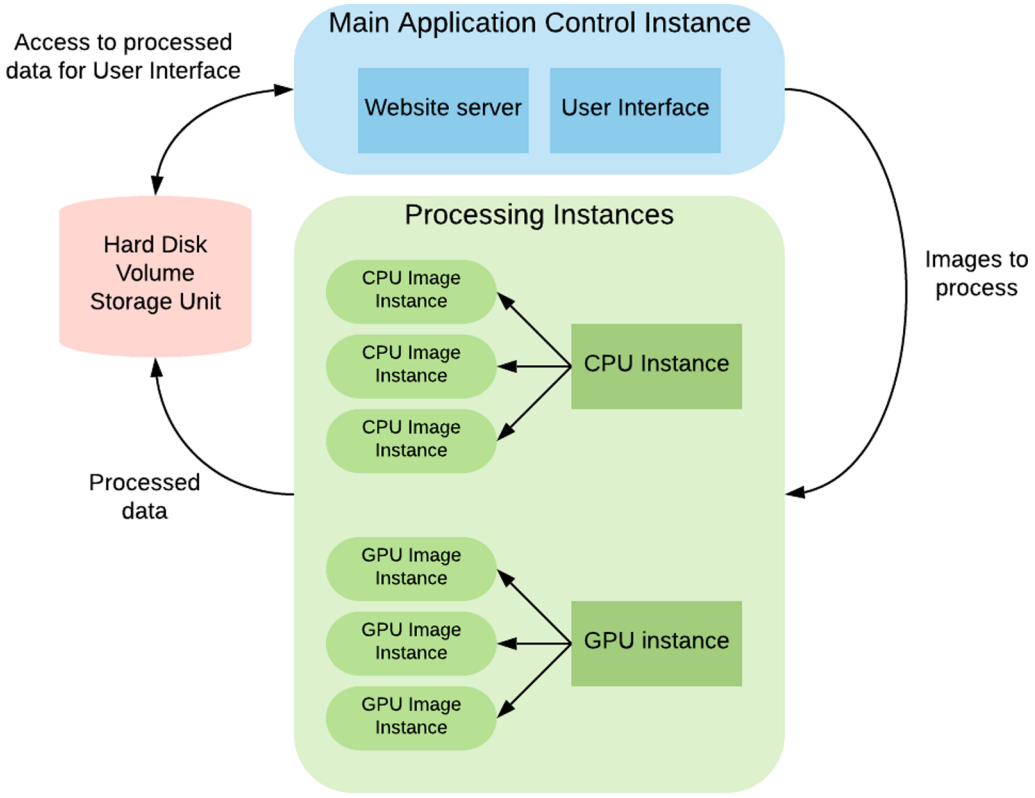

Fig. 1. Workflow of the Amazon Web Services (AWS) system.

algorithm. With the processing finished, the GPU image instance is closed, and the resulting data are stored in the volume unit to be accessed by the website for display in the user interface. Fig. 1 shows the workflow of the AWS system created.

2.3. Tree detection algorithm

The orthomosaic is processed by an algorithm developed in C in multiple steps (Fig. 2) in order to output: (i) individual tree and tree gap (skip) detection, (ii) tree height, (iii) tree canopy area estimation (iv) tree health/stress estimation (among other information). The methodology adopted in this study is an improvement of a methodology described in Ampatzidis and Partel (2019). Briefly, the algorithm runs a first CNN tree detection on the map and process its output to analyze the field's row orientation patterns and to estimate distances between trees and between rows. Then, based on the field geometry, the algorithm makes assumptions of probable tree locations, and uses this information to run a second classificator CNN based on the previous detected positions.

The first difference between the original methodology (Ampatzidis and Partel, 2019) and this study is the use of a low-cost RGB camera for image acquisition (and target detections), instead of using more expensive multispectral cameras. Furthermore, instead of a YOLO (Redmon and Farhadi, 2018) algorithm (adopted by Ampatzidis and Partel, 2019), this proposed methodology uses a Faster R-CNN algorithm (Ren et al., 2015) for the first CNN tree detection. Contrary to YOLO, the Faster R-CNN is not suitable for real-time applications, but usually yield better accuracy in object detection problems. The Faster R-CNN is a Region Proposal Network (RPN), composed of two steps: (i) development of a bounding-box for each object in the image; and (ii) feature extraction of the region of interest (ROI) of each bounding-box for a final classification. ResNet101 network was chosen empirically, among different networks, after preliminary experiments. The second CNN runs a YOLO classificator using the Darknet19 network on locations, based on the detected field geometry.

The first step of this "tree detection" procedure is to gather image data from an orchard using UAVs (or similar aerial or ground platforms). With the images from the UAV flight, the user can choose to process the raw images in a software of his choice to generate the orthomosaic, or to upload the raw images directly to the Agroview website for processing using the cloud-based engine to generate the orthomosaic map. The engine software used to generate the orthomosaic map in the proposed cloud-based application is an open source toolkit named Open Drone Map (ODM), version 0.3.1, running on Ubuntu 16.04. The ODM supports as inputs JPEG images from the UAV cameras and generates an orthorectified image and a DSM using structure from motion techniques (Turner et al., 2012). The DSM contains the height information of the area flown (Fig. 3). After uploading, the orthomosaic of the area flown will be available in the cloud for the next step. Fig. 4 shows the workflow for the data acquisition and upload process of the website.

When the orthomosaic is available in the cloud, the user has another manual input: (i) develop the region of interest, which represents the area where the user is interested in running the tree detection algorithm (aka, field boundaries). This step includes a tool that allows the user to select blank areas inside of the region for the algorithm to skip/ignore (Fig. 5), such as lakes or buildings.

After the manual inputs, the orthomosaic map goes through a preprocessing step of color calibration based on the RGB average levels of the original image using histogram equalization (Cheng and Shi, 2004). This preprocessing calibration reduces variations from different RGB cameras, as each camera has its own calibration of color, exposure and saturation. Hence, this preprocessing step can increase the effectiveness of the CNN model developed. Fig. 6 shows this transformation applied to an orthomosaic.

After the preprocessing step, the first detection algorithm runs (Fig. 5) to find an initial number of trees and uses this information to identify rows orientation. With the information of each row, the second

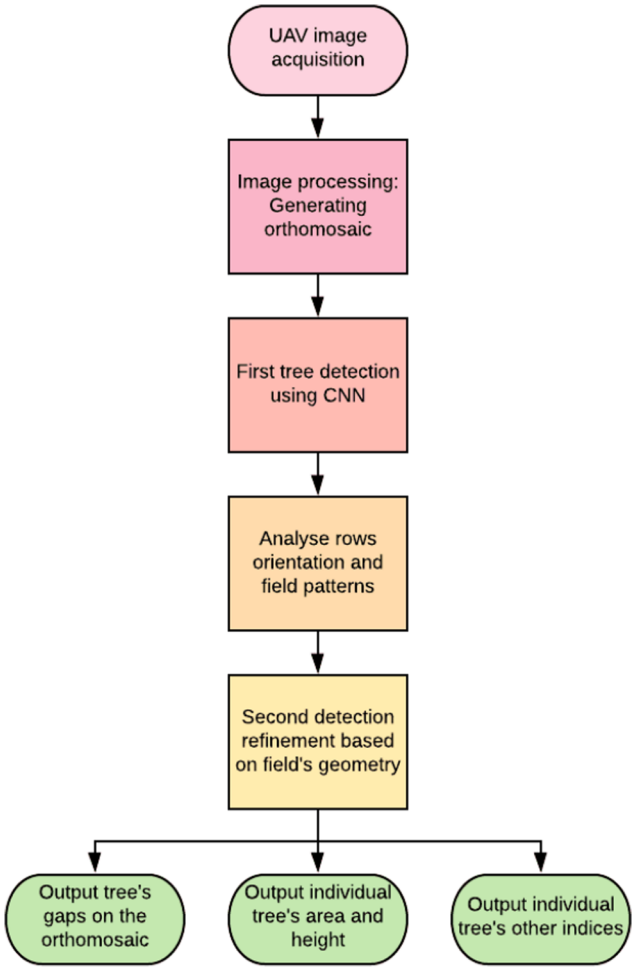

Fig. 2. Workflow of the smart and automated tree detection algorithm (Ampatzidis and Partel, 2019).

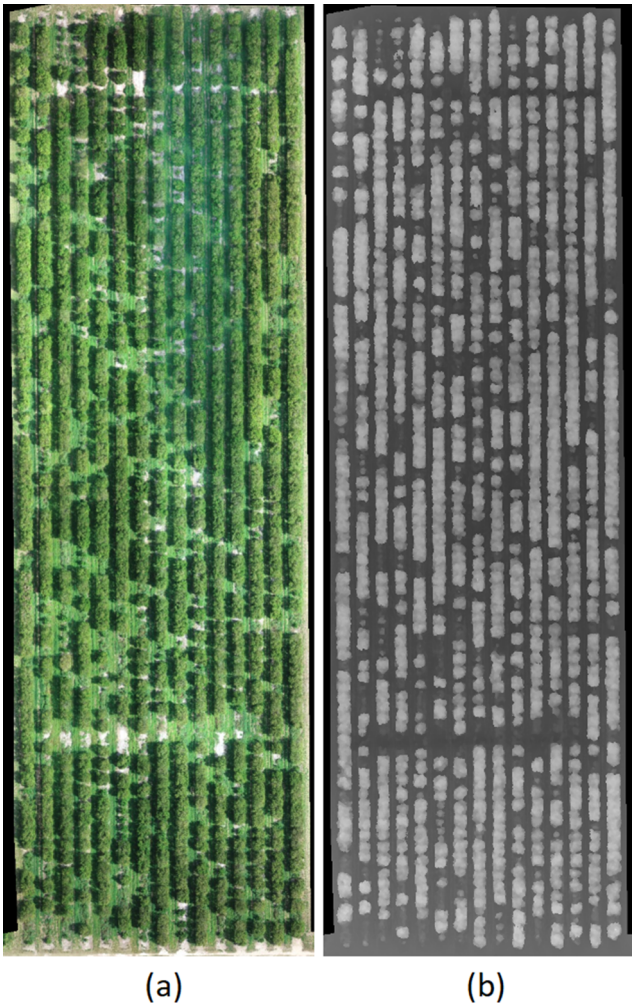

Fig. 3. Citrus grove block generated by the Open Drone Map (ODM) engine: a) Orthomosaic map, and b) DSM.

CNN classificator runs along each row for a more precise detection. The final data is returned to the user in the cloud. Fig. 7 presents the workflow of the entire process for using the cloud-based algorithm.

In the final processed map, when a user selects ("clicks") a field (e.g., citrus orchard), a window with some field analytics (e.g., total number of tree and tree gap counts, field size, average values of tree height and canopy area, etc.) is displayed (Fig. 8a). For more information about this field, the user has to click the "View Block" button (Fig. 8a-left). Then, a new map is presented with tree and tree gap detections (Fig. 8b). This interactive Agroview application allows the user to select to display 2–4 different categories based on tree height, canopy size, and tree health (Fig. 8b-left). The tree health indices were developed based on Costa et al. (2020). Moreover, the user can select to display on the map only trees that belong to a specific category; for example, all trees with less than 7 ft height. The user can do that by unselecting the other categories in the provided histogram (Fig. 8b-left). The total number of trees that belong to a specific category can be found by selecting a category on the provided histogram.

3. Experimental design

To evaluate the accuracy of the developed cloud-based technology, several experiments were conducted in a commercial citrus orchard in Hendry County, Florida (26.6557 N, 81.2891 W) (Fig. 9), in February 2019. The orchard comprised multiple blocks of Hamlin and Valencia citrus varieties on a wide range of ages and sizes; all trees were over one year old and over 1 m tall, which was a favorable condition for this experiment, as it reduces the problem of detecting very small trees (less than 1 m tall). The experiments were divided into: (i) evaluation of detected number of trees and gaps (locations with no trees or dead trees), and (ii) evaluation of detected tree height and canopy area. The evaluation of the developed plant health (or stress) indices is presented in Costa et al. (2020); this Agroview technology utilizes the same methodology to generate the heath maps.

3.1. Evaluation of detected number of trees and tree gaps

The proposed algorithm was evaluated in terms of number of trees and gaps detected for 39 different citrus blocks (1,871 acres) (Table 2). A manual count of the number of trees (ground truth) was performed on each block by trained farm crew members, by driving within the rows and using a handheld manual counting device. The ground truth number of gaps was estimated for each block by subtracting the count of trees from the total spaces of that block. The blocks were divided into: (i) normal tree spacing (blocks 1–23), where the block spacing was 7.8 × 3.6 m, and (ii) high density spacing (blocks 24–39), where the spacing was 7.2 × 2.3 m (Table 2). The UAV data of all 39 blocks were processed in the developed cloud-based software, and the obtained results of trees and gap counts were compared to the manually measured numbers.

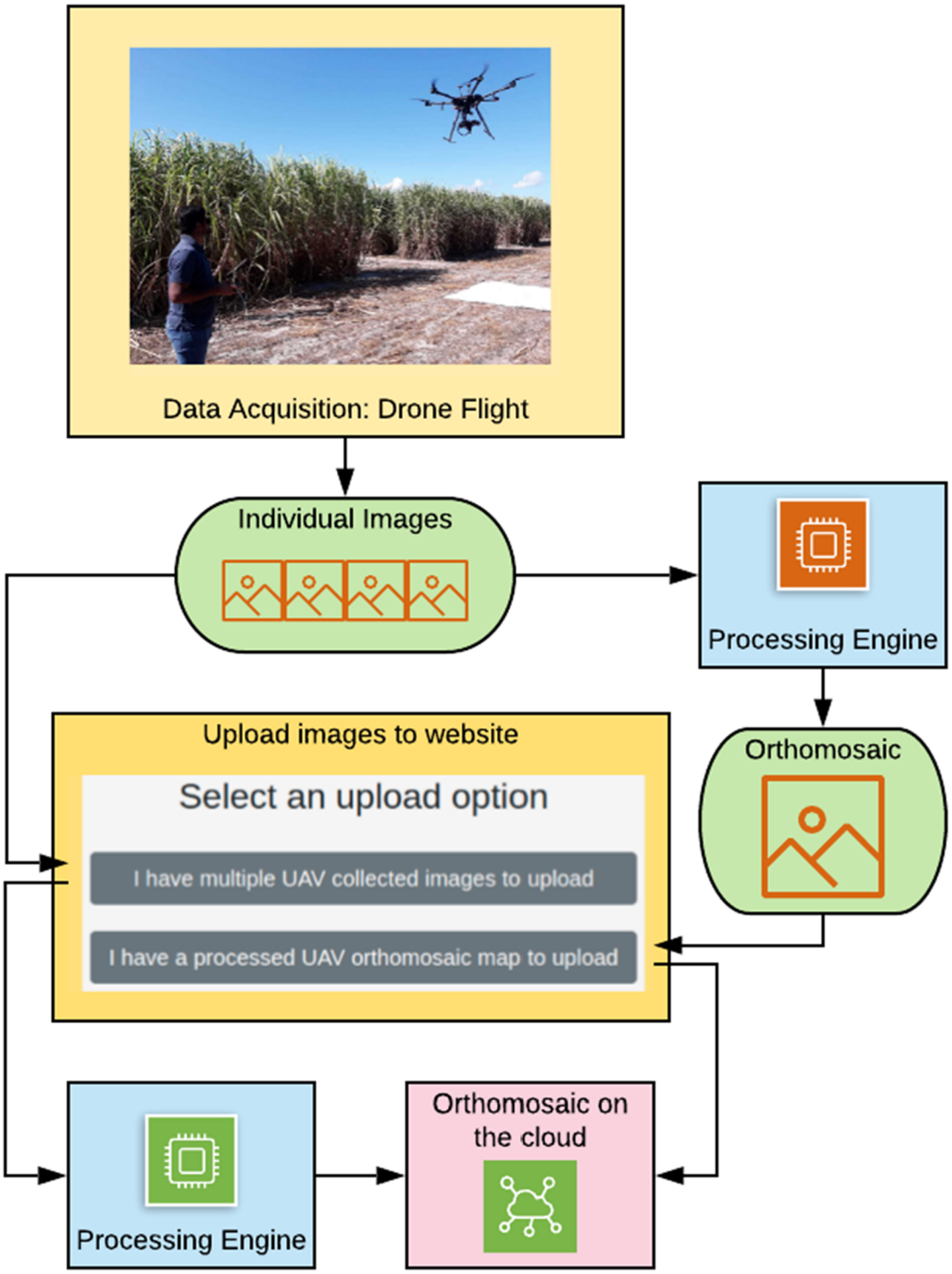

Fig. 4. Workflow of the data acquisition from UAVs and image upload process to the Agroview website.

3.2. Evaluation of estimated tree height and canopy area

To evaluate the estimated (predicted) values of tree height and canopy area, a subset of 100 trees were selected and manually measured on the field using measuring poles and tapes. Two blocks were randomly chosen, and 50 trees were selected from each block to be manually measured. The trees were randomly selected from different rows spread across the blocks. One block (block 8) includes trees with normal spacing, and another block (block 25) includes high-density spacing trees (Table 3). The canopy area measurement (manually measured) was defined to be the area of a rectangle enclosing the canopy. Although this definition overestimates the real tree canopy area, it was selected, as it is a common practice followed by the citrus growers.

3.3. Evaluation metrics

3.3.1. Mean absolute percentage error (MAPE)

The Mean Absolute Percentage Error (MAPE) is a statistical tool that represents the error between a forecast and the ground truth value,

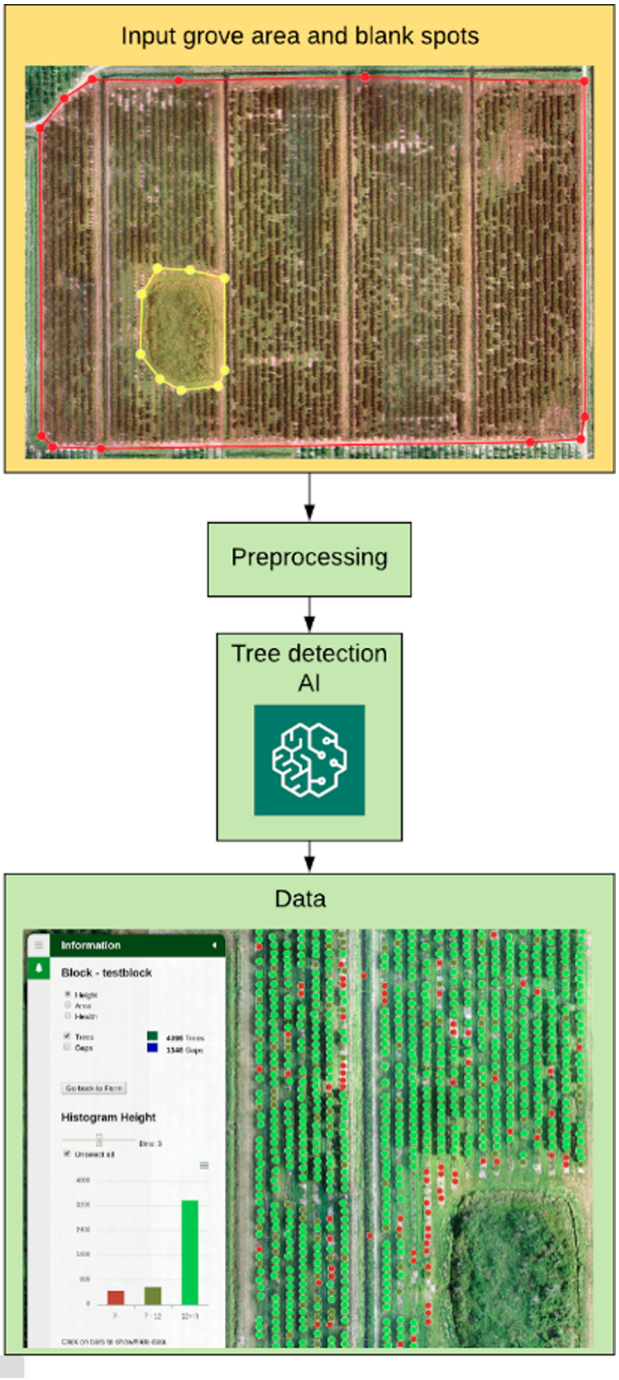

Fig. 5. Algorithm workflow that presents the user manual inputs step, the color calibration preprocessing step, the tree detection algorithm, and the generation of the final data (dots represent plants; in this map, three colored dots present three tree height categories).

which in this study are the algorithm's predictions and the manual measurements, respectively. It is given by the absolute difference between measurements, divided by the ground truth value, which results in a percentage.

3.3.2. Measure of agreement

Agreement between measurements refers to the degree of concordance between two sets of measurements of the same individual by two different methodologies. Statistical methods to test agreements are used to decide whether one technique for measuring a variable can substitute another (Ranganathan et al., 2017). Observations of two different methods are often inappropriately evaluated for agreement using the Pearson correlation coefficient, which is an incorrect measure of reproducibility or repeatability (Watson and Petrie, 2010). The Pearson correlation is heavily dependent on the dataset itself; for example, one or few outliers may introduce a false sense of relationship (Aggarwal and Ranganathan, 2016).

One of the techniques for agreement measurement is the Bland and Altman diagram (Bland and Altman, 1999). This diagram is a display of the pattern and agreement of one variable being measured by two different methodologies (Watson and Petrie, 2010). In this study, the methodologies compared are the manual methods (e.g., for tree counts, tree height and canopy area measurements) and the estimations by the algorithm. The Bland and Altman diagram plots the difference between a pair of measurements on the vertical axis and the mean value of the pair on the horizontal axis. Since the variability of the dataset is small (e.g., tree count, height and area are similar to all individuals), we can express this difference in pairs by percentage, by dividing all values by the mean of each measurement.

To determine the repeatability, the method assumes a normal distribution of differences, where 95% of them are expected to lie between $d \pm 1.96s$, where d is the mean of observed differences and s is the standard deviation. When compared to a ground truth method, such as the manual method for measuring trees, the value of upper and lower limits with 95% probability is an acceptable statistical value of certainty and reproducibility for the measurement technique, which can then be compared between other studies as it is not heavily dependent on the dataset itself.

4. Results and discussion

After the data acquisition procedures, the data were processed on the cloud to generate the results. The total processing time (to generate the final results) was on average 120 min for a 60 acres block, being around 90% of the time (108 min) on the orthomosaic processing and development (stitching), and only 10% (12 min) for the preprocessing, processing, tree detection, tree canopy measurements, and data visualization.

4.1. Evaluation of tree and tree gap detection and counting

The detected number of trees and gaps, and the manual counted number are presented in Tables 4 and 5, divided as normal spacing blocks and high-density spacing blocks, respectively. The results show a MAPE of 2.29% and 4.23% for tree and tree gap counts, respectively, on the normal spacing blocks, and 4.50% and 9.17%, respectively, for the high-density spacing blocks. The difference in error from the two blocks categories is significant, around double for both trees and gaps count on the high-density blocks. Trees close packed have more overlapping canopies which has shown to be harder to distinguish and accurately count, thus the difference in accuracy. Errors on gap counts were greater than tree count errors on the majority of blocks (normal and high-density spacing). This greater error is produced due to missed gaps on the field boundaries; based on the field boundaries, the algorithm predicts the beginning of a tree row and the location of its first tree (or gap). Since, it is difficult to accurately define the field boundaries on a map, the algorithm might produce more errors in the beginning of each row (especially if the boundaries are not well defined by the user).

It must be noted that in this experiment there were no recently planted trees; the youngest trees were 2 to 3 years old. The presence of recently planted trees would certainly decrease the accuracy as small trees (less than 1 m tall) are harder to detect. For example, it is difficult to distinguish young trees from weeds, especially when the weeds have the same height with the young trees. This threshold of size and age for accurate young tree detection will be further investigated in future studies.

The overall MAPE achieved for tree count prediction was 3.18%

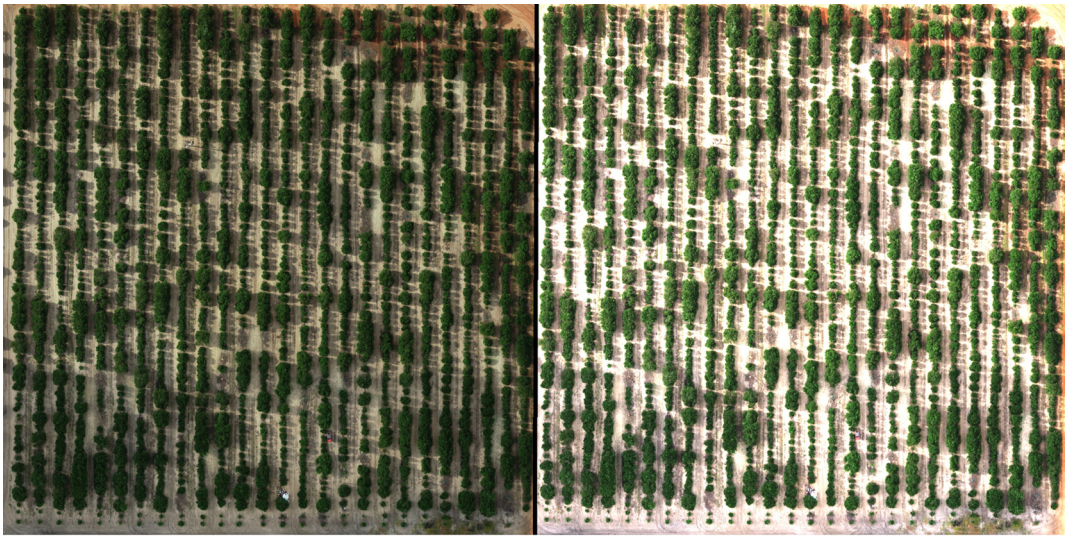

Fig. 6. a) Generated orthomosaic map, and b) color calibration preprocessed map.

(97% accuracy), and for tree gap prediction was 6.86% (93% accuracy). Currently, there are limited studies on individual tree detection for citrus. Csillik et al. (2018) reported an accuracy of 96% in detecting 2,912 individual trees using a simple convolutional neural network and a refinement algorithm based on super-pixels. Osco et al. (2020) proposed a methodology using a CNN to generate confidence maps for canopy occurrence and achieved 95% accuracy evaluating around 3,735 trees in a high-density citrus orchard. In a previous study that shared some of the methodology proposed in this research, Ampatzidis and Partel (2019) achieved an overall 99.8% accuracy, evaluated on a relatively uniform and small citrus field (14 acres with 4,931 trees). In the present study, a more complete and user-friendly workflow was evaluated over a large citrus farm (175,977 trees; 1,871 acres; 39 citrus blocks) comprising normal and high-density spaced trees. The evaluated area and number of trees were significantly larger than other studies. Robustness and generality are important features on any remote sensing technique to effectively incorporate this technology into agricultural management.

The Bland and Altman diagram for tree counts is presented in Fig. 10. A range of ± 0.12 was achieved, which means that the proposed technology has a 95% probability to detect and count trees with a maximum error of 12%. However, Fig. 10 clearly shows that most of the detections were between the range of ± 0.05 error. This indicates a high probability for the algorithm to count trees with under 5% error.

A reliable and effective assessment of tree inventory on an orchard is critical also for crop insurance purposes. Natural disasters, such as hurricanes in Florida, can cause severe crop damage and insurance claims. Quickly estimating this damage can improve the management of insurance resources. After hurricane Irma in 2017 in Florida, the United State Department of Agriculture (USDA) through the Risk Management Agency developed new insurance policies, requiring growers to create and submit accurate tree inventories for all perennial tree policies that change insurance or experience a significant increase or decrease in coverage each year. Currently, most citrus growers in Florida hire consulting companies to manually count trees, which is a very time consuming and labor intensive operation, since workers need to drive throughout the fields to manually count and categorize trees (using clickers or other counting devices). This manual procedure can

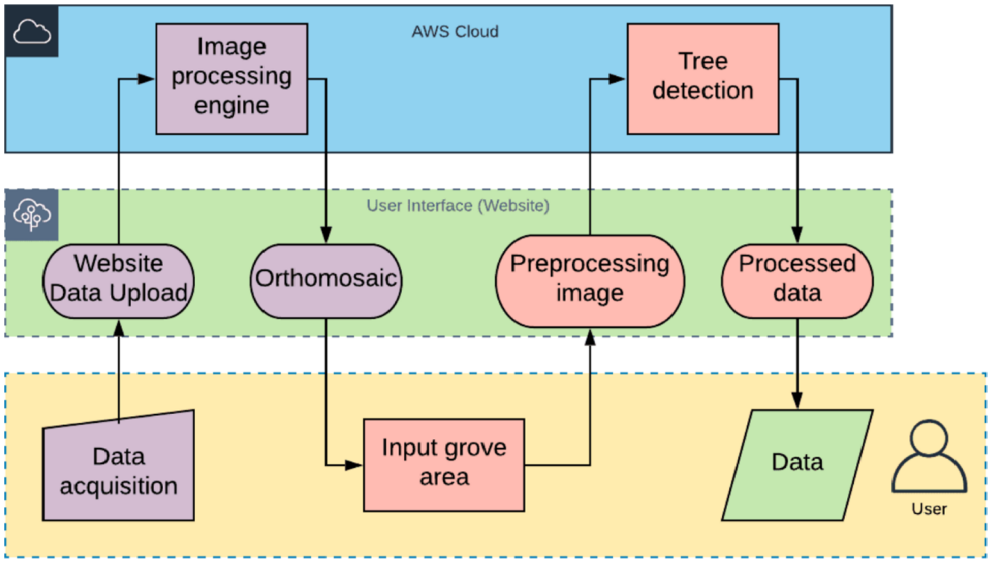

Fig. 7. Workflow of the entire process for the cloud-based application (Agroview).

Fig. 8. User interface to visualize data for: (a) multiple blocks (average field statistics for each block), and (b) individual field and tree information (e.g., tree categories based on height or canopy size).

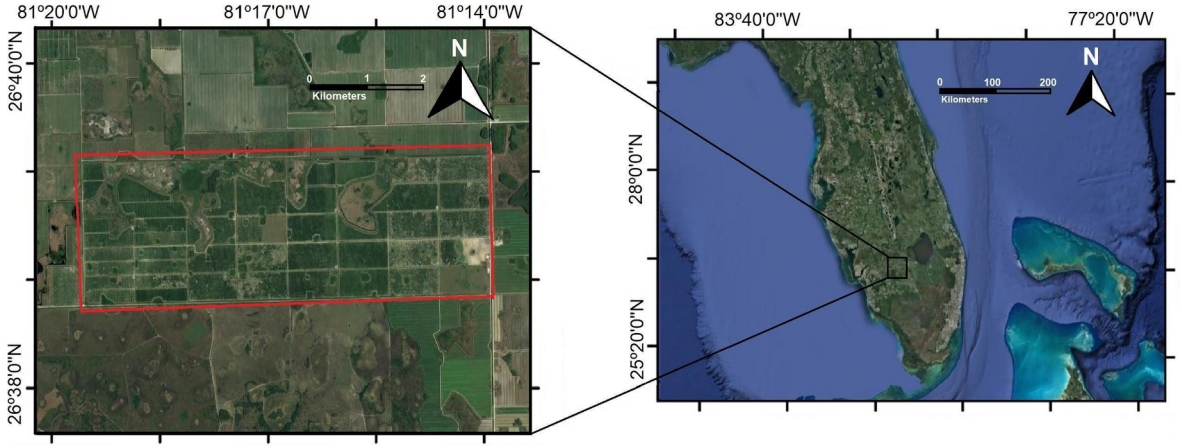

Fig. 9. Citrus farm, containing 39 citrus blocks, in Hendry County, Florida, where the evaluation experiments were conducted.

Table 2
Citrus blocks selected for tree detection and count evaluation; blocks marked with (*) indicate high-density tree spacing blocks. The normal tree spacing was 7.8 × 3.6 m, and the high density spacing was 7.2 × 2.3 m.

Block	Area (acres)	Block	Area (acres)	Block	Area (acres)
1	73.3	*15*	32.2	*29**	35.5
2	66.7	*16*	70.3	*30**	50.1
3	64.7	*17*	61.5	*31**	43.4
4	71.2	*18*	84.3	*32**	27.1
5	73.8	*19*	70.2	*33**	30
6	71.6	*20*	63.6	*34**	28
7	66.4	*21*	31.2	*35**	35.2
8	73	*22*	14.7	*36**	36
9	38.9	*23*	39.4	*37**	18.7
10	48.2	*24**	34.3	*38**	15
11	65.2	*25**	36	*39**	18.5
12	72.6	*26**	32.9		
13	67.6	*27**	27.4	Total	1871.2
14	51.9	*28**	30.6		

Table 3
Blocks selected to evaluate the performance of the proposed algorithm to estimate tree height and canopy area.

Block	Area (acres)	Selected Trees	Spacing
8	73	50	Normal
25	36	50	High-density

cost up to $12–14/acre and takes 2–4 weeks to count trees in 1,000 acres. Citrus growers usually create tree inventories every 12–36 months, based on their management practices (e.g., re-planting) or incidences of natural disaster events. The proposed UAV-based novel technology, Agroview, can be used to develop tree inventories and save the Florida citrus industry (among other industries all over the world) at least 70% of the data collection cost, and 90% of the data collection time.

4.2. Evaluation of tree height and canopy area estimation

A total of 100 trees were selected and their height and canopy area manually measured from (i) block 8 (normal spacing), and (ii) block 25 (high-density spacing). These manual measurements were compared to the estimations by the proposed cloud-based algorithm. Results are presented in Figs. 11–13. The MAPE on height and canopy area for block 8 were 4.47% and 13.88%, respectively. Block 25 (high-density) obtained a MAPE of 12.93% and 34.46% for tree height and canopy area, respectively. Ampatzidis and Partel (2019) reported a MAPE of 14.50% for canopy area estimation on a normal spacing grove, which is very close to the obtained MAPE for block 8 (13.88%). The obtained tree height and canopy area error were significantly higher for the high-density block. This difference in errors, especially for the canopy area, is due to the less clear canopy delineation on the high-density block. Errors on tree height estimations were found to be mainly due to lack of key points on the orthomosaic stitching process. This issue will be further investigated in future research.

For block 8, the Bland and Altman diagram for tree height (Fig. 12a) presents a range of ± 0.09,which means that the reliability of the measurement for the tree canopy height is within 9% error, and for the tree canopy area (Fig. 12b) presents a range of 35%. The larger range of error for the area measurement shows that delineating tree canopies (especially high-density ones) is harder than estimating the tree height.

The Bland and Altman diagram for the measurements of block 25 are presented in Fig. 13a (tree canopy height) and Fig. 13b (tree canopy area). For the tree height, it shows a range of reliability of 21%, which is accurate for most purposes. The range for tree canopy area is not so accurate as the trees are closely packed and can confuse the algorithm on where the delimitation is for each tree.

5. Conclusion

Precise and efficient crop management in orchards depends on methods to detect and assess individual trees. A cloud- and AI-based technique (Agroview application) was developed to automatically process, analyze, and visualize UAV collected data for individual tree monitoring and assessment. This interactive application comprised a machine vision algorithm (AI-based) that uses deep learning to effectively detect individual plants on aerial maps. An experiment conducted on a large commercial citrus orchard (175,977 trees; 1,871 acres; normal and high density spacing) achieved an overall tree detection error of 2.29%. The Agroview estimated tree height and canopy area

Table 4
Comparison between the algorithm's tree and tree gap detections and manual counts in blocks with normal spacing (7.8 × 3.6 m).

Block	Detected Trees	Detected gaps	Counted trees	Counted gaps	Error trees	%	Error gaps	%
1	4907	4899	5032	5230	125	2.48%	331	6.33%
2	4432	4418	4523	4815	91	2.01%	397	8.25%
3	4309	4331	4406	4652	97	2.20%	321	6.90%
4	6397	3305	6244	3724	153	2.45%	419	11.25%
5	4394	5690	4395	5937	1	0.02%	247	4.16%
6	3238	6116	3180	6844	58	1.82%	728	10.64%
7	4679	4544	4487	4809	192	4.28%	265	5.51%
8	4715	5228	4681	5539	34	0.73%	311	5.61%
9	2139	3282	2135	3311	4	0.19%	29	0.88%
10	3127	3335	3158	3590	31	0.98%	255	7.10%
11	7055	2120	7030	2098	25	0.36%	22	1.05%
12	7011	3032	7050	3114	39	0.55%	82	2.63%
13	5532	3871	5300	4164	232	4.38%	293	7.04%
14	3138	3825	3131	4135	7	0.22%	310	7.50%
15	2334	2132	2348	2160	14	0.60%	28	1.30%
16	4816	4892	5162	4680	346	6.70%	212	4.53%
17	5531	3101	5693	2917	162	2.85%	184	6.31%
18	7336	4307	7309	4493	27	0.37%	186	4.14%
19	4181	5436	4220	5608	39	0.92%	172	3.07%
20	4503	4277	4511	4393	8	0.18%	116	2.64%
21	2476	1878	2400	1968	76	3.17%	90	4.57%
22	916	1005	1002	1056	86	8.58%	51	4.83%
23	2717	2746	2888	2628	171	5.92%	118	4.49%
					MAPE	2.29%		4.23%

Table 5
Comparison between the algorithm's tree and tree gap detections and manual counts in high-density spacing (7.2 × 2.3 m).

Block	Detected Trees	Detected gaps	Counted trees	Counted gaps	Error trees	%	Error gaps	%
24	7130	1690	7268	1393	138	1.90%	297	21.32%
25	2828	5825	3128	5962	300	9.59%	137	2.30%
26	3745	4181	3971	4336	226	5.69%	155	3.57%
27	3431	4715	3625	4682	194	5.35%	33	0.70%
28	3050	4928	3251	4476	201	6.18%	452	10.10%
29	7107	1720	6970	1994	137	1.97%	274	13.74%
30	9771	2711	9493	3157	278	2.93%	446	14.13%
31	9355	1679	9254	1705	101	1.09%	26	1.52%
32	2003	4547	2173	4386	170	7.82%	161	3.67%
33	2739	4592	2939	4491	200	6.81%	101	2.25%
34	2657	4048	2827	4243	170	6.01%	195	4.60%
35	5956	2761	5768	3120	188	3.26%	359	11.51%
36	4995	3805	5064	4026	69	1.36%	221	5.49%
37	3104	1545	3019	1703	85	2.82%	158	9.28%
38	3252	733	3141	647	111	3.53%	86	13.29%
39	3584	1125	3801	870	217	5.71%	255	29.31%
					MAPE	4.50%		9.17%

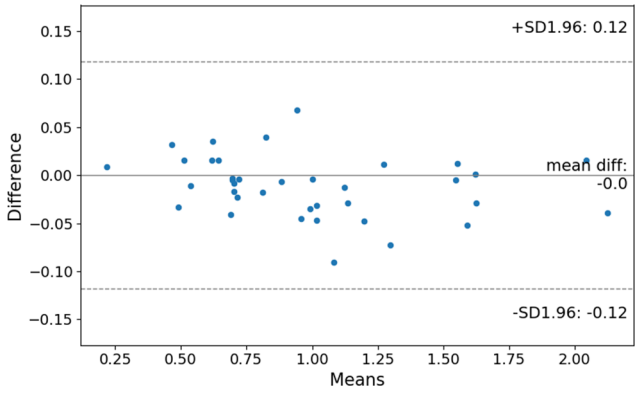

Fig. 10. Bland and Altman diagram for the tree detection and count of the 39 studied citrus blocks.

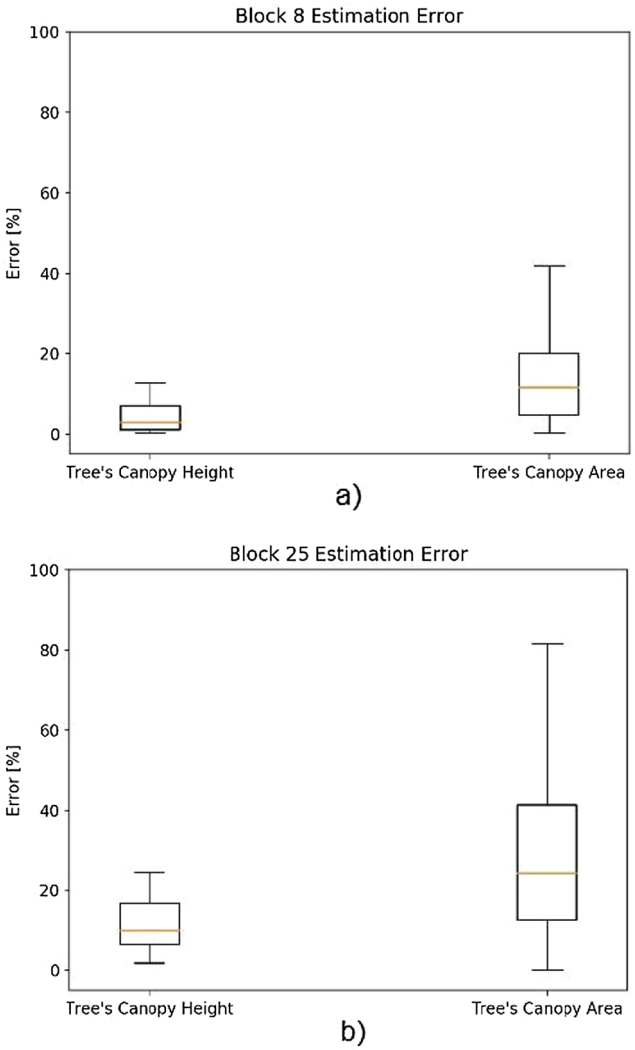

Fig. 11. Error for tree height and canopy area prediction for: a) block 8 (normal spacing), and b) block 25 (high density spacing).

with high accuracy too. The proposed user-friendly application has a great potential to provide individual plant analysis over large areas and to compare phenotypic characteristics on different sets of plants. Recently, USDA developed new insurance policies, requiring growers to create and submit accurate tree inventories for all perennial tree policies. Traditional manual tree count techniques are very labor-intensive, time-consuming, and expensive (cost of around $12–24/acre; can take 2–4 weeks to cover 1,000 acres). The developed Agroview application can create accurate tree inventories in sort time and save the Florida tree industry (among other industries all over the world) at least 70% of the data collection cost, and 90% of the data collection time.

CRediT authorship contribution statement

Yiannis Ampatzidis: Conceptualization, Methodology, Validation, Formal analysis, Data curation, Writing - original draft, Writing - review & editing, Visualization, Supervision, Project administration, Funding acquisition. **Victor Partel:** Conceptualization, Methodology, Software, Validation, Formal analysis, Data curation, Writing - original draft, Visualization. **Lucas Costa:** Methodology, Validation, Formal analysis, Data curation, Writing - original draft, Visualization.

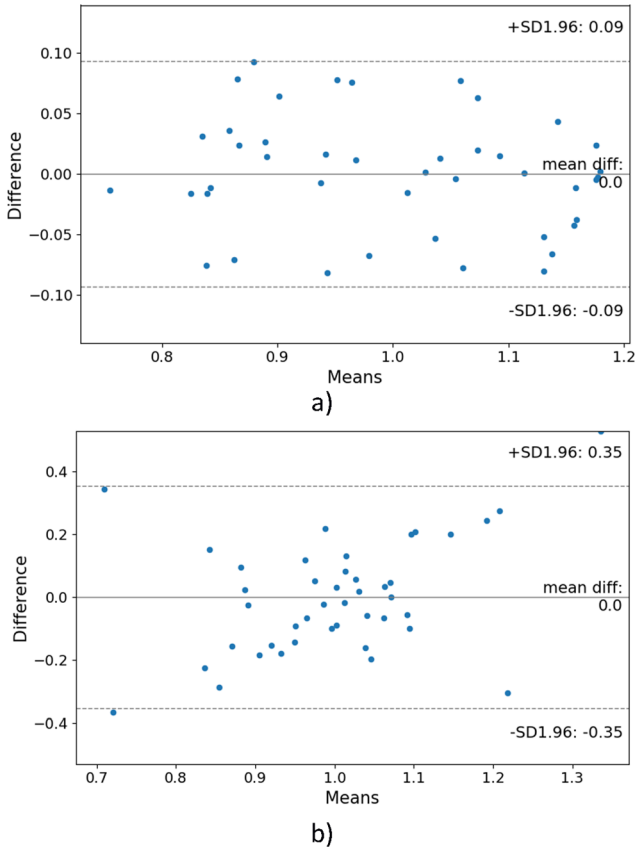

Fig. 12. Bland and Altman diagram error in percentage for block 8 (normal spacing) for estimating: a) tree canopy height, and b) tree canopy area.

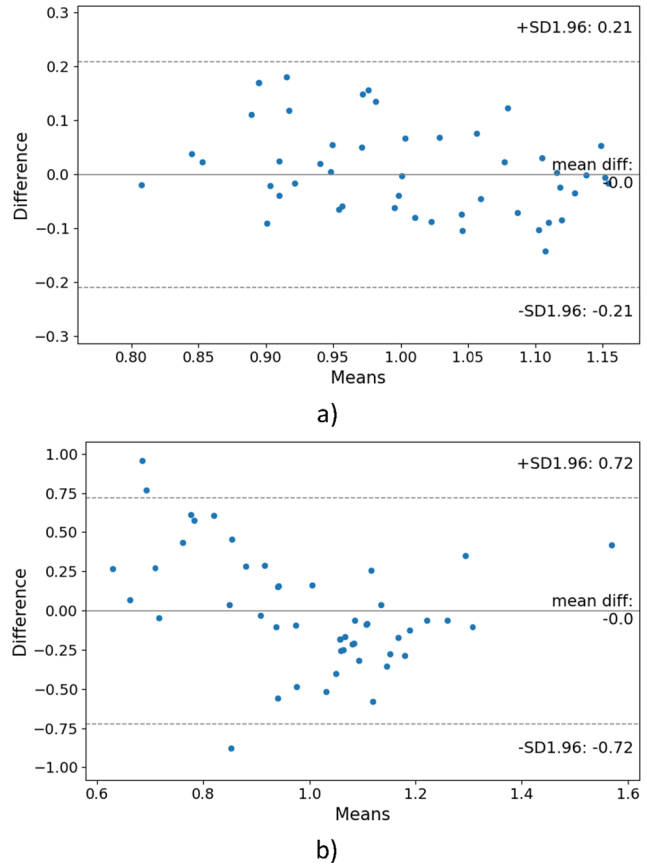

Fig. 13. Bland and Altman diagram error in percentage for block 25 (high-density spacing) for estimating: a) tree canopy height, and b) tree canopy area.

Declaration of Competing Interest

The authors declare that they have no known competing financial interests or personal relationships that could have appeared to influence the work reported in this paper.

Acknowledgement

This material was made possible, in part, by a Cooperative Agreement from the U.S. Department of Agriculture's Animal and Plant Health Inspection Service (APHIS). Its contents are solely the responsibility of the authors and do not necessarily represent the official views of the USDA.

Appendix A. Supplementary material

Supplementary data to this article can be found online at https://doi.org/10.1016/j.compag.2020.105457.

References

Abdulridha, J., Ehsani, R., Abd-Elrahman, A., Ampatzidis, Y., 2019a. A Remote Sensing technique for detecting laurel wilt disease in avocado in presence of other biotic and abiotic stresses. Comput. Electron. Agric. 156, 549–557.

Abdulridha, J., Ampatzidis, Y., Kakarla, S.C., Roberts, P., 2019b. Detection of target spot and bacterial spot diseases in tomato using UAV-based and benchtop-based hyperspectral imaging techniques. Precis. Agric. (November), 1–24.

Abdulridha, J., Batuman, O., Ampatzidis, Y., 2019c. UAV-based remote sensing technique to detect citrus canker disease utilizing hyperspectral imaging and machine learning. Remote Sens. 11 (11), 1373.

Aggarwal, R., Ranganathan, P., 2016. Common pitfalls in statistical analysis: The use of correlation techniques. Perspect. Clin. Res. 7 (4), 187.

Ampatzidis, Y., De Bellis, L., Luvisi, A., 2017. iPathology: robotic applications and management of plants and plant diseases. Sustainability 9 (6), 1010. https://doi.org/10.3390/su9061010.

Ampatzidis, Y., Partel, V., 2019. UAV-based High Throughput phenotyping in citrus utilizing multispectral imaging and artificial intelligence. Remote Sens., 11(4), 410, doi:10.3390/rs11040410.

Ampatzidis, Y., Partel, V., Meyering, B., Albrecht, U., 2019. Citrus Rootstock Evaluation Utilizing UAV-based Remote Sensing and Artificial Intelligence. Comput. Electron. Agric. 164, 104900. https://doi.org/10.1016/j.compag.2019.104900.

Bland, J.M., Altman, D.G., 1999. Measuring agreement in method comparison studies. Stat. Methods Med. Res. 8 (2), 135–160.

Buyya, R., Broberg, J., Goscinski, A.M., (Eds.), 2010. Cloud computing: Principles and Paradigms, vol. 87, John Wiley & Sons.

Cheng, H.D., Shi, X.J., 2004. A simple and effective histogram equalization approach to image enhancement. Digital Singal Processing 14 (2), 158–170.

Costa, L., Nunes, L., Ampatzidis, Y., 2020. A new visible band index (vNDVI) for estimating NDVI values on RGB images utilizing genetic algorithms. Comput. Electron. Agric. 172, 105334.

Cruz, A., Ampatzidis, Y., Pierro, R., Materazzi, A., Panattoni, A., De Bellis, L., Luvisi, A., 2019. Detection of grapevine yellows symptoms in Vitis vinifera L. with artificial intelligence. Comput. Electron. Agric. 157, 63–76.

Cruz, A.C., Luvisi, A., De Bellis, L., Ampatzidis, Y., 2017. X-FIDO: An effective application for detecting olive quick decline syndrome with novel deep learning methods. Frontiers, Plant Sci., 10 October 2017, doi:10.3389/fpls.2017.01741.

Csillik, O., Cherbini, J., Johnson, R., Lyons, A., Kelly, M., 2018. Identification of citrus trees from unmanned aerial vehicle imagery using convolutional neural networks. Drones 2 (4), 39. https://doi.org/10.3390/drones2040039.

Das, U., 2018. Precision farming a promising technology in horticulture: A review. Int. J. Pure Appl. Biosci. 2018 (6), 1596–1606.

Dong, X., Zhang, Z., Yu, R., Tian, Q., Zhu, X., 2020. Extraction of information about individual trees from high-spatial-resolution UAV-acquired images of an orchard. Remote Sens. 12, 133. https://doi.org/10.3390/rs12010133.

Garcia-Ruiz, F., Sankaran, S., Maja, J.M., Lee, W.S., Rasmussen, J., Ehsani, R., 2013. Comparison of two aerial imaging platforms for identification of Huanglongbing-infected citrus trees. Comput. Electron. Agric. 91, 106–115.

Ghatrehsamani, S., Wade, T., Ampatzidis, Y., 2018. The adoption of precision agriculture technologies by Florida growers: a comparison of 2005 and 2018 survey data. In: XXX International Horticultural Congress, II International Symposium on Mechanization, Precision Horticulture, and Robotics, 12-16 August, 2018, Istanbul Turkey.

Harihara, J., Fuller, J., Ampatzidis, Y., Abdulridha, J., Lerwill, A., 2019. Finite difference analysis and bivariate correlation of hyperspectral data for detecting laurel wilt disease and nutritional deficiency in avocado. Remote Sens., 11(15), 1748, doi:10.3390/rs11151748.

Hayes, B., 2008. Cloud computing. Commun. ACM 51 (7), 9–11.

Hunt Jr., E.R., Hively, W.D., Fujikawa, S.J., Linden, D.S., Daughtry, C.S.T., McCarty, G.W., 2010. Acquisition of nir-green-blue digital photographs from unmanned aircraft for crop monitoring. Remote Sens. 2, 290–305.

Jiménez-Brenes, F.M., López-Granados, F., Castro, A.I., Torres-Sánchez, J., Serrano, N., Peña, J.M., 2017. Quantifying pruning impacts on olive tree architecture and annual canopy growth by using UAV-based 3D modelling. Plant Methods 13, 55.
Jinesh, V., 2011. Best practices in architecting cloud applications in the AWS cloud. Cloud Computing: Principles and Paradigms, vol. 18, 459–490.
Krizhevsky, A., Sutskever, I., Hinton, G.E., 2012. Imagenet classification with deep convolutional neural networks. Adv. Neural Informat. Proces. Syst. 1097–1105.
Kussul, N., Mykola, L., Skakun, S., Shelestov, A., 2017. Deep learning classification of land cover and crop types using remote sensing data. IEEE Geosci. Remote Sens. Lett. 14 (5), 778–782. https://doi.org/10.1109/LGRS.2017.2681128.
Luvisi, A., Ampatzidis, Y., De Bellis, L., 2016. Plant pathology and information technology: opportunity and uncertainty in pest management. Sustainability 8 (8), 831. https://doi.org/10.3390/su8080831.
Mahlein, A.K., 2016. Plant disease detection by imaging sensors — parallels and specific demands for precision agriculture and plant phenotyping. Plant Dis 100, 241–251.
Maillard, P., Gomes, M.F., 2016. Detection and counting of orchard trees from vhr images using a geometrical-optical model and marked template matching. In: Proceedings of the ISPRS Annals of the Photogrammetry, Remote Sensing and Spatial Information Sciences, Prague, Czech Republic, 12–19 July 2016; III-7, pp. 75–82.
Malek, S., Bazi, Y., Alajlan, N., AlHichri, H., Melgani, F., 2014. Efficient Framework for Palm Tree Detection in UAV Images. IEEE J. Sel. Top. Appl. Earth Observat. Remote Sens. 7, 4692–4703.
Matese, A., Capraro, F., Primicerio, J., Gualato, G., Di Gennaro, S.F., Agati, G., 2013. Mapping of vine vigor by UAV and anthocyanin content by a non-destructive fluorescence technique. Precis. Agric. 13, 201–208.
Mu, Y., Fujii, Y., Takata, D., Zheng, B., Noshita, K., Honda, K., Ninomiya, S., Guo, W., 2018. Characterization of peach tree crown by using high-resolution images from an unmanned aerial vehicle. Hortic. Res. 5, 74.
Fawcett, D., Azlan, B., Hill, T.C., Kho, L.K., Bennie, J., Anderson, K., 2019. Unmanned aerial vehicle (UAV) derived structure-from-motion photogrammetry point clouds for oil palm (Elaeis guineensis) canopy segmentation and height estimation. Int. J. Remote Sens. 40, 1–23.
Ok, A.O., Ozdarici-Ok, A., 2017. Detection of citrus trees from UAV DSMs. In: Proceedings of the ISPRS Annals of the Photogrammetry, Remote Sensing and Spatial Information Sciences, Hannover, Germany, 6–9 June 2017, 4, pp. 27–34.
Osco, L.P., de Arruda, M.D.S., Junior, J.M., da Silva, N.B., Ramos, A.P.M., Moryia, É.A.S., et al., 2020. A convolutional neural network approach for counting and geolocating citrus-trees in UAV multispectral imagery. ISPRS J. Photogramm. Remote Sens. 160, 97–106.
Pajares, G., 2015. Overview and current status of remote sensing applications based on unmanned aerial vehicles (UAVs). Photogramm. Eng. Remote Sens. 81, 281–330.
Panda, S.S., Hoogenboom, G., Paz, J.O., 2010. Remote sensing and geospatial technological applications for site-specific management of fruit and nut crops: A review. Remote Sens. 2, 1973–1997.
Partel, V., Nunes, L., Stansley, P., Ampatzidis, Y., 2019a. Automated vision-based system for monitoring Asian citrus Psyllid in orchards utilizing artificial intelligence. Comput. Electron. Agric. 162, 328–336.
Partel, V., Kakarla, S.C., Ampatzidis, Y., 2019b. Development and evaluation of a low-cost and smart technology for precision weed management utilizing artificial intelligence. Comput. Electron. Agric. 157, 339–350.
Ranganathan, P., Pramesh, C.S., Aggarwal, R., 2017. Common pitfalls in statistical analysis: Measures of agreement. Perspect. Clin. Res. 8 (4), 187.
Redmon, J., Farhadi, A., 2018. Yolov3: An incremental improvement. arXiv preprint arXiv:1804.02767.
Ren, S., He, K., Girshick, R., Sun, J., 2015. Faster r-cnn: Towards real-time object detection with region proposal networks. In Advances in neural information processing systems (NIPS 2015), 91–99.
Romero-Trigueros, C., Nortes, P.A., Alarcón, J.J., Hunink, J.E., Parra, M., Contreras, S., Nicolás, E., 2017. Effects of saline reclaimed waters and deficit irrigation on Citrus physiology assessed by UAV remote sensing. Agric. Water Manag. 183, 60–69.
Salamí, E., Gallardo, A., Skorobogatov, G., Barrado, C., 2019. On-the-fly olive tree counting using a UAS and cloud services. Remote Sens. 11, 316.
Sarron, J., Malézieux, É., Sané, C.A.B., Faye, É., 2018. Mango yield mapping at the orchard scale based on tree structure and land cover assessed by UAV. Remote Sens. 10, 1900.
Shakoor, N., Lee, S., Mockler, T.C., 2017. High throughput phenotyping to accelerate crop breeding and monitoring of diseases in the field. Curr. Opin. Plant Biol. 38, 184–192.
Singh, A., Ganapathysubramanian, B., Singh, A.K., Sarkar, S., 2016. Machine learning for high-throughput stress phenotyping in plants. Trends Plant Sci. 21, 110–124.
Torres-Sánchez, J., López-Granados, F., Serrano, N., Arquero, O., Peña, J.M., 2015. High-throughput 3-D monitoring of agricultural-tree plantations with Unmanned Aerial Vehicle (UAV) technology. PLoS One 10, e0130479.
Turner, D., Lucieer, A., Watson, C., 2012. An automated technique for generating georectified mosaics from ultra-high resolution unmanned aerial vehicle (UAV) imagery, based on structure from motion (SfM) point clouds. Remote Sens. 4 (5), 1392–1410.
Villamizar, M., Garces, O., Ochoa, L., Castro, H., Salamanca, L., Verano, M., et al., 2016. Infrastructure cost comparison of running web applications in the cloud using AWS lambda and monolithic and microservice architectures. In: 2016 16th IEEE/ACM International Symposium on Cluster, Cloud and Grid Computing (CCGrid), pp. 179–182.
Watson, P.F., Petrie, A., 2010. Method agreement analysis: a review of correct methodology. Theriogenology 73 (9), 1167–1179.
Zhang, X., Derival, M., Albrecht, U., Ampatzidis, Y., 2019. Evaluation of a ground penetrating radar to map root architecture of HLB-infected citrus trees. Agronomy (Special Issue: Precision Agr.) 9 (7), 354. https://doi.org/10.3390/agronomy9070354.